7.6 SMALL SCALE TURBULENCE MODULATION BY DUCTED GRAVITY WAVES ABOVE THE NOCTURNAL BOUNDARY LAYER

Yannick P. Meillier*, Rod G. Frehlich, R. Michael Jones, Ben B. Balsley
University of Colorado, Boulder, Colorado

1. INTRODUCTION

The motivation for studying the nocturnal boundary layer (NBL) is driven by the need for improving the accuracy of current atmospheric models. Modern numerical weather prediction models use the Monin-Obhukov similarity theory (see, e.g. Chen et al. 1997) to estimate surface fluxes of heat, moisture, and momentum. Under the typical stable conditions of a nocturnal boundary layer, theory breaks down because of the characteristic intermittency of turbulence (e.g., Mahrt 1989). Improvement of numerical weather prediction models requires a more complete understanding of both the properties and the dynamical processes that influence the NBL structure and morphology, especially the properties and role of turbulence intermittency.

Ways by which the turbulence field can be altered by mesoscale systems such as gravity waves have been well documented (e.g. Einaudi and Finnigan 1981; Finnigan and Einaudi 1981; Finnigan et al. 1984; Sun et al. 2004). Following the early work of Finnigan et al. (1984), a few theoretical studies tried to relate the changes of turbulence intensity to a time-varying gradient Richardson number (Fual et al. 1982; Weinstock 1987; Chimonas 1972; Kondo et al. 1978; Edwards and Mobbs 1997). However, this idea is often not well accepted since "turbulence is considered as a random, three-dimensional state of motion governed mainly by the non-linear terms of the equations of motion […]. A linearized wave description of the motion is impossible […], and a deterministic approach is often abandoned with attention being confined to the statistical properties of the flow" (Gossard 1975). Yet, theoretical studies examined this possibility and the basic ideas underlying wave-turbulence coupling are summarized as follow: 1) the occurrence of turbulence can be related to the local, wave-modulated, Richardson number (Ri); 2) turbulence occurs with a mean and a periodic component; 3) turbulence extracts energy from the wave, limiting its growth (Fua et al. 1982). Accurate measurement of fine-scale turbulence is difficult and the proposed theories need to be validated by experimental data.

In this paper, we discuss some aspects of the data acquired with the turbulence probes of the CIRES Tethered Lifting System (TLS) during the sixth Intensive Operation Period (IOP6) of the CASES-99 field campaign. Periodic occurrences of turbulence intensity enhancements, in both the temperature structure constant (C_T^2) and energy dissipation rate (ε) time series, are analyzed and correlated with fluctuations of the background temperature and velocity signals. The purpose of this paper is to present experimental evidence of the validity of the idea of a 'deterministic approach of turbulence intermittency'.

2. THE TETHERED LIFTING SYSTEM (TLS)

The CIRES Tethered Lifting System was designed to perform fine-scale measurements of temperature and velocity, which are converted to turbulence statistics (C_T^2 and ε) anywhere from ground up to a few kilometers high. The system consists of a kite (or a blimp depending on the wind conditions) that can loft an array of turbulence payloads. The TLS can either be operated in a constant altitude mode, to record time series of various quantities at a fixed point in space, or it can perform successive ascents and descents to produce profile measurements (e.g., see Balsley et al. 1998). Each turbulence package measures the temperature and velocity fluctuations at a sampling rate of 200 Hz with fast response fine-wire cold-wire (CW) and hot-wire (HW) sensors. For calibration purposes, 1-second data of temperature and velocity are also archived by each turbulence payload using respectively a solid-state temperature sensor and a Pitot-tube vaned into the wind. Each turbulence probe also records 1 Hz data of wind direction (magnetic compass), pressure (piezo-electric pressure sensor), and the pitch, roll, and yaw angles (three-

* *Corresponding author address:* Yannick Meillier, Cooperative Institute for Research in the Environmental Sciences (CIRES), 216 UCB, University of Colorado, Boulder, CO 80309-0216; e-mail: yannick.meillier@colorado.edu.

axis tilt sensor). Finally, a basic meteorological payload (BMP) is also used to archive 1-second values of temperature, humidity, pressure, wind speed and wind direction, as well as various "housekeeping" data.

The absolute accuracy of the temperature measurements is better than 0.5 K while the accuracy of the linear calibration constant is better than 2%. For velocity, the absolute accuracy is better than 1ms^{-1} and the accuracy of the slope of the calibration curve is better than 5%. C_T^2 and ε are computed by fitting the temperature and velocity spectra to a theoretical model that captures the Kolmogorov microscale and the –5/3 slope of the inertial range. The accuracy of those spectral levels is typically 15% with 1-second data intervals (for more details see Frehlich et al. 2003).

2. MEAN STATE EVOLUTION

Profiles before and after the constant altitude region (~465 m AGL) of the 4.2-5.2 UTC time period provide information on the evolution of the background conditions. The early potential temperature profile (2.1-2.8 UTC ascent) exhibits a uniform, weakly stratified layer extending from 50m to 650m AGL ($d\theta/dz$~1.6 C/km), surrounded by steep temperature inversions (Fig.1). With time, stratification of the residual layer strengthens and reaches ~37 C/km at 6.1 UTC. Accompanying this increasing stratification is a drop of the capping inversion altitude, from ~650 m at 2.1 UTC, down to ~500 m at 6.1 UTC and thereafter.

The velocity profiles exhibit a broad nocturnal jet from 50 m to 200 m AGL, coupled with a strong shear below it. The jet maximum increases with time, from 10 m/s at 2.1 UTC to 12.5 m/s at 6.1 UTC. Above the jet, velocity gradually decreases with altitude (down to 6 m/s at the capping inversion for the 2.1 UTC profile, down to 8 m/s at 6.1 UTC) and from the upper levels, high altitude winds of roughly 10 m/s seem to be traveling their way down, from 750 m AGL at 2.1 UTC, to 550 m AGL at 6.1 UTC. Wind directions are nearly uniform throughout the residual boundary layer. Initially pointing toward the west direction at the beginning of IOP6, winds experience an anticyclonic rotation and point toward the northwest by about 8.0 UTC (Fritts et al. 2003).
Last but not least, Richardson number profiles show that early on, shear-generated turbulence is possible at the height of 465 m AGL as Ri<0.25 in this region (Fig.2). However, throughout the night, the stability profile evolves and at 6.1 UTC, a stable region settles in at this same height (Ri$\rightarrow\infty$).

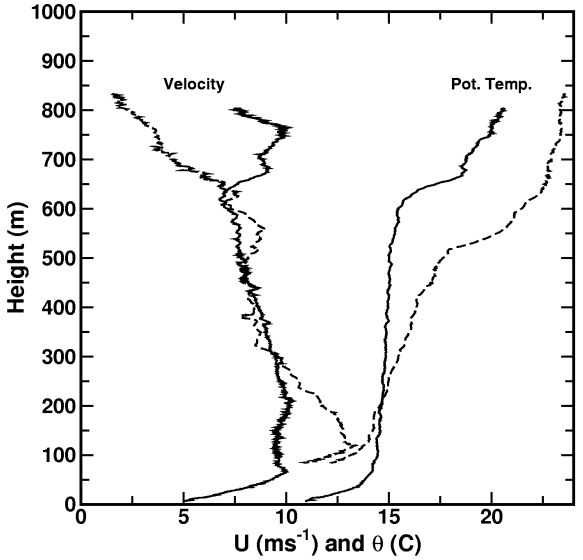

Figure 1. Potential temperature and velocity profiles from the 2.1-2.8 UTC ascent (solid line), and the 5.7-6.1 UTC descent (dashed).

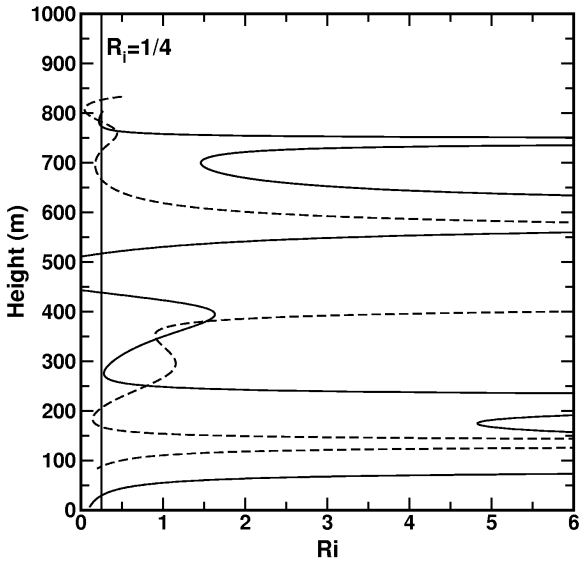

Figure 2. Richardson number profiles from the 2.1 UTC ascent (solid line), and the 6.1 UTC descent (dashed line).

3. WAVE SIGNATURES

Time series of the hot-wire velocity and cold-wire temperature for the constant altitude region of 4.3 to 5.4 UTC are shown in figure 3. Both signals exhibit sustained wave-like fluctuations throughout the hour-long observation period. The corresponding spectral densities feature a well-

defined peak at a frequency of 0.0037 Hz, and mean amplitudes of 0.2 m/s and 0.2 °C.

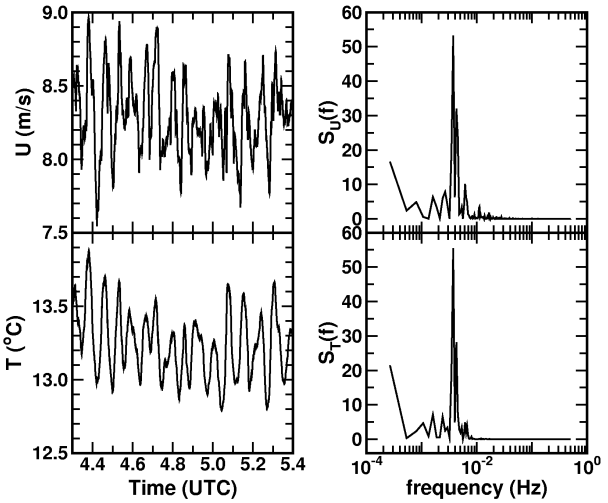

Figure 3. Time series and spectra of CW Temperature and HW Velocity from 4.3 to 5.4 UTC.

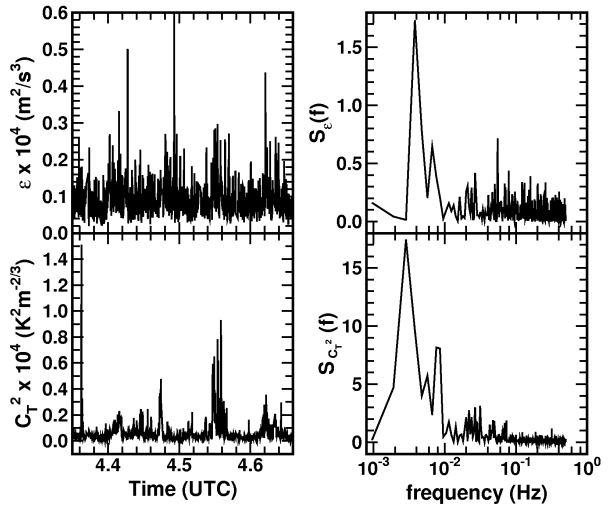

Figure 4. Time series and spectra of C_T^2 and ε from 4.35 to 4.66 UTC.

Similar plots of C_T^2 and ε for a subset of the constant altitude region display the typical characteristic of turbulence intermittency i.e., sporadic bursts of turbulence gathered in patches that seem to be randomly distributed in time (Fig.4). However, on closer investigation, regions of turbulence enhancement appear to be periodically distributed in time with the same characteristic frequency as the frequency of oscillation of the temperature and velocity waves. This is best evidenced by the spectral densities of C_T^2 and ε (Fig.4) and to a lesser extent, the time series of Log(C_T^2) and Log(ε) (Fig5).

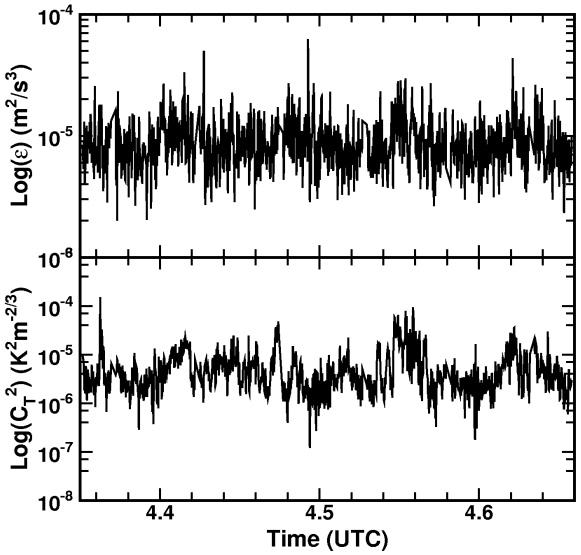

Figure 5. Time series of Log(C_T^2) and Log(ε) from 4.35 to 4.66 UTC.

Phase speed and direction of propagation are two quantities that are hard to deduce from the TLS data. Attempts were made to compute these two quantities using the impedance equation (Gossard 1975) with the TLS pressure and velocity data:

$$C_P = \frac{1}{\rho}\frac{A_P}{A_U}$$

where A_p and A_u the amplitudes of the pressure and velocity waves respectively in Pa and m/s. Although a realistic value of phase speed was found using this technique (C_P~20 m/s), the results highly depend on the accuracy of the estimates of the pressure and velocity waves amplitude. Although the amplitude of the velocity wave is rather accurate, estimating the pressure amplitude from the noisy TLS pressure sensor is more challenging and bounding the accuracy of this estimate is difficult. Fortunately, other instruments of the CASES-99 campaign also monitored this same wave event. Measurements of u', w', and T' from the Wyoming King Air (Atmospheric Technology Division, NCAR. http://flights.uwyo.edu) yielded estimates of the phase speed (C_x>10 m/s), of the apparent horizontal wavelength (λ~1-3 km), and of the direction of wave propagation (~westward) (Fritts et al. 2003).

Finally an analysis of the sensor package motion was performed to identify other possible sources

of waves. Although results of this study are not presented in this paper, it was determined that the waves that were recorded by the TLS sensors are true atmospheric waves and not the result of package and kite oscillations (e.g., periodic altitude fluctuations of the TLS sensors through a region of sheared velocity and sheared temperature would artificially generate waves in the temperature and velocity signals).

4. WAVE-TURBULENCE INTERACTIONS

"A gravity wave propagating through a stable atmosphere in which the gradient Richardson number approaches, but is larger than the critical value of ¼, will inevitably perturb the background wind and temperature structure of the medium, and will therefore disturb the stability and turbulence intensity of the flow as the Richardson number is periodically forced below its critical value of ¼" (Gossard 1975). This concept forms the basis of this study to investigate correlations between the changes of turbulence intensity and the periodic fluctuations of a wave-modulated Richardson number.

Wave-like fluctuations of potential temperature and velocity will generate a fluctuating component of the Richardson number only if the waves have tilted phase fronts with height or if the amplitude of the fluctuations are a function of altitude. The wave event studied in this paper was identified as a phenomenon of gravity wave ducting by Fritts et al. (2003), which rules out the first potential source of fluctuating gradients of velocity and potential temperature. For the second scenario, investigating whether or not the amplitudes of the ducted waves of potential temperature and velocity change with height around 465 m AGL requires solving the Taylor-Goldstein (TG) equation (Gossard 1975; Gill 1982), which describes the vertical structure of gravity waves, i.e.,

$$\frac{\partial^2 w}{\partial z^2} + m^2 w' = 0$$

where 'm^2' is the Scorer parameter,

$$m^2 = \frac{N^2}{(u_0 - C_P)^2} - \frac{\partial^2 u_0 / \partial z^2}{u_0 - C_P} - k^2 - 2\Gamma \frac{\partial u_0 / \partial z}{u_0 - C_P} - \Gamma^2$$

'Γ' the Eckhart coefficient,

$$\Gamma = \frac{1}{2}\left(\frac{g}{C_S^2} - \frac{N^2}{g} \right)$$

k the horizontal wave number, u_0 the background velocity in the direction of wave propagation, C_P the wave phase speed, and C_s the sound speed. Modal solutions of the TG equation are computed with the "matrix method" (Monserrat 1996), which assumes solutions of the form:

$$w(z,t) = W(z) e^{i(k\,x\,-\,\omega\,t)}$$

Given the input profiles of background temperature and velocity and given an estimate for the horizontal wave number, the matrix method automatically returns the complete set of modal solutions $W(z)$: each modal solution having a unique phase speed and frequency. Note that the matrix method will return numerous spurious modal solutions that need to be ruled out from the final set of modal solutions. A common rule of thumb for identifying those spurious modes is to check for the presence of critical layers within the duct region, i.e. regions where the mode's phase speed equals the background velocity at some height within the duct. Solutions that involve critical layers are rejected because the TG equation is not valid when critical layers are present. Given this selection criterion, multiple runs performed with different values of 'k' resulted in the emergence of a single dominant mode. Note that the frequency of the dominant mode changed with every run, which permits the calculation of the wave number '$k = 2\pi / \lambda$' required for the frequency of the modal solution to match the measured wave frequency of 0.0037 Hz. A value for λ of 3.75 km was found which is close to what was proposed by Fritts et al. (2003) who assumed a value in the range of 1 to 3 km.

Profiles of the W modal solution and of its corresponding Scorer parameter for λ=3.75 km are shown in figure 6. Modal solutions of the horizontal velocity and potential temperature fields are then related to the modal solutions of the vertical velocity field by (Newsom and Banta 2003):

$$U = iW \frac{\partial u_0}{\partial z} \left[k(u_0 - C_P) \right]^{-1}$$

$$\Theta = iW \frac{\partial \theta_0}{\partial z} \left[k(u_0 - C_P) \right]^{-1}$$

where U, W, and Θ are the amplitudes of the modal solutions of u, w, and θ. A Taylor series expansion is then used to compute the Richardson number as a function of time and height. For x = 0:

$$u = u_0 + u' = u_0 + U\, e^{-i\,\omega\,t} = u_0 + \mathrm{Re}[U] \sin(\omega\, t)$$

$$\theta = \theta_0 + \theta' = \theta_0 + \Theta\, e^{-i\,\omega\, t} = \theta_0 + \mathrm{Re}[\Theta]\sin(\omega\, t)$$

and the Taylor series expansion of Ri is

$$Ri = g\,\frac{\partial\theta_0/\partial z}{\theta_0\,(\partial u_0/\partial z)^2}\left[1 - \frac{\theta'}{\theta_0} - 2\,\frac{\partial u'/\partial z}{\partial u_0/\partial z} + \frac{\partial\theta'/\partial z}{\partial\theta_0/\partial z}\right]$$

which yields

$$Ri = g\,\frac{\partial\theta_0/\partial z}{\theta_0\,(\partial u_0/\partial z)^2}\left[1 - \left(\frac{\Theta}{\theta_0} + 2\,\frac{\partial U/\partial z}{\partial u_0/\partial z} - \frac{\partial\Theta/\partial z}{\partial\theta_0/\partial z}\right)\sin(\omega\, t)\right]$$

which can be written as

$$Ri = g\,\frac{\partial\theta_0/\partial z}{\theta_0\,(\partial u_0/\partial z)^2}\left[1 - A\sin(\omega\, t)\right]$$

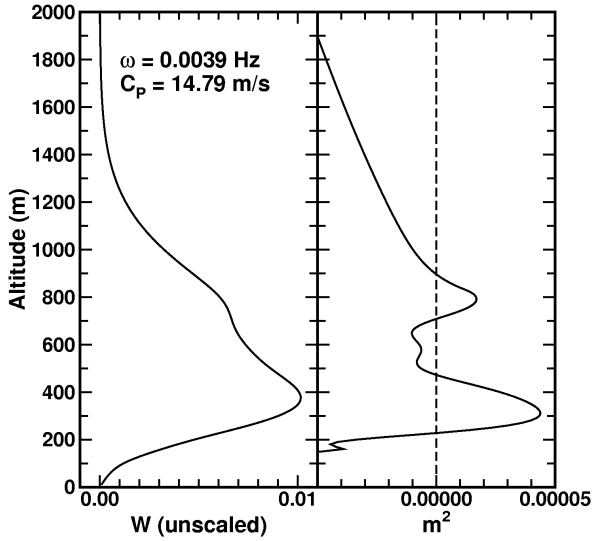

Figure 6. Dominant modal solution and corresponding Scorer parameter for the w field.

Depending on the sign of 'A', the fluctuating component of the Richardson number will either be in phase with the waves of velocity and potential temperature (A<0) or out phase (A>0). Regions of enhanced turbulence in the time series of section 3 appear to be matched with troughs of the u and θ waves, and therefore, if those bursts of turbulence are correlated with a fluctuating Richardson number, we should expect the wave component of Ri to be in phase with the waves of velocity and potential temperature. Computations show that at 465 m AGL, the fluctuating Ri is indeed in phase with u' and θ' which agrees with the TLS turbulence measurements.

REFERENCES

Balsley, B.B., M. L. Jensen, and R. G. Frehlich, 1998: The use of state-of-the-art kites for profiling the lower atmosphere. *Bound.-Layer Meteor*, **87**, 1-25.

Chen, F., Z. Janjic, and K. Mitchell, 1997: Impact of atmospheric surface-layer parameterization in the new land-surface scheme of the NCEP mesoscale Eta Model. Bound.-Layer-Meteor., **85**, 391-421.

Chimonas, G, 1972: The stability of a coupled wave-turbulence system in a parallel shear flow. Bound.-Layer Met., **2**, 444-452.

Edwards, N.R., and S. D. Mobbs, 1997: Observations of isolated wave-turbulence interactions in the stable atmospheric boundary layer. Quart. J. R. Met. Soc., **123,** 561-584.

Einaudi F., and J.J. Finnigan,1981: The interaction between an internal gravity wave and the planetary boundary layer. Part I: The linear analysis. Quart. J. R. Met. Soc., **107**, 793-806.

Finnigan, J.J., and F. Einaudi, 1981: The interaction between an internal gravity wave and the planetary boundary layer. Part II: Effect of the wave on the turbulence structure. Quart. J. R. Met. Soc., **107**, 807-832.

Finnigan, J.J., F. Einaudi, and D. Fua, 1984: The interaction between an internal gravity wave and turbulence in the stably-stratified nocturnal boundary layer. JAS, **41**, no16 (Aug.), 2409-2436.

Frehlich, R.G, Y. Meillier, M. Jensen, B. Balsley, 2003: Turbulence measurements with the CIRES Tethered Lifting System during CASES-99: Calibration and Spectral Analysis of Temperature and Velocity. JAS, **60** (Oct.), 2487-2495.

Fritts, C. et al., 2003: Analysis of ducted motions in the stable nocturnal boundary layer during CASES-99. JAS, **60** (Oct.), 2450-2471.

Fua, D., G. Chimonas, F. Einaudi, and O. Zeman, 1982: An analysis of wave-turbulence interaction. JAS, **39** (Nov.), 2450-2463.

Gill, A. 1982: Atmosphere-Ocean Dynamics. International Geophysics Series, v30. Academic Press.

Gossard, E.E., and W.H. Hooke, 1975: Waves in the atmosphere. Elsevier Scientific publishing company, Developments in atmospheric science, 2.

Kondo, J., O. Kanechikam and N. Yaruda, 1978: Heat and momentum transfer under strong stability in the atmospheric surface layer. JAS, **35**, 1012-1021.

Mahrt, L., 1989: Intermittency of atmospheric turbulence, JAS, **46**, no1 (Jan.), 79-95.

Monserrat, S., A.J. Thorpe, 1996: Use of ducting theory in an observed case of gravity waves. JAS, **53** (Jun.), no12, 1724-1736.

Newsom, R.K., and R.M. Banta, 2003: Shear-flow instability in the stable nocturnal boundary layer as observed by Doppler Lidar during CASES-99. JAS, **60** (Jan.), 16-33.

Sun, J. et al. 2004: Atmospheric disturbances that generate intermittent turbulence in nocturnal boundary layers. Bound.-Layer Met., **110**, 255-279.

Weinstock, J., 1987: The turbulence field generated by a linear gravity wave. JAS, **44**, no2 (Jan.), 410-420.